THE APPLICATION OF CFD FOR MILITARY AIRCRAFT DESIGN AT TRANSONIC SPEEDS

C. W. Smith
W. W. Braymen
I. C. Bhateley
W. K. Londenberg
General Dynamics
Forth Worth Division
Ft. Worth, TX

ABSTRACT

Numerous computational fluid dynamics (CFD) codes are available that solve any of several variations of the transonic flow equations from small disturbance to full Navier-Stokes. The design philosophy at General Dynamics Fort Worth Division involves use of all of these levels of codes, depending on the stage of configuration development. Throughout this process, drag calculation is a central issue.

This paper provides an overview of several transonic codes and presents representative test-to-theory comparisons for fighter-type configurations. Correlations are shown for lift, drag, pitching moment, and pressure distributions. The future of applied CFD is also discussed, including the important task of code validation. With the progress being made in code development and the continued evolution in computer hardware, we can look forward to routine application of these codes for increasingly more complex geometries and flow conditions.

INTRODUCTION

It seems ironic -- the transonic flow regime is the most difficult for the aerodynamicist to analyze, but is the part of the flight envelope most critical to design success of military aircraft and fighters in particular. Calculating transonic characteristics with regions of mixed subsonic and supersonic flows, embedded shocks, and viscous interactions becomes complex even for simple geometries. When these complexities are combined with the need to consider complete configurations with blended wing/bodies, multiple lifting surfaces of low-aspect ratio, moderate-to-high sweep, high taper, leading- and trailing-edge flaps, and external stores, not to mention propulsion-induced aerodynamic interactions, the problem becomes overwhelming. Nevertheless, significant advancements have been made in CFD during the past ten years. Numerous codes are now available that solve any of several variations of the transonic flow equations from small disturbance to full Navier-Stokes. Solutions for simple to quite complex shapes can be obtained for a wide range of geometries modeled by these codes. Obviously, the more complex the flow algorithm or geometry, the more intensive the computation and associated computer time.

Cost has dictated that practicality be an important consideration in the selection of design tools. Evidence of this is the fairly common preliminary design practice of employing linear theory or modified-linear theory at transonic speeds where linear theory is clearly not applicable. This points to the need for transonic codes to be computationally efficient for routine use. Otherwise, they can never be employed in a design optimization study such as that required for an aeroelastically tailored wing, a process that often requires iteration of several thousand geometry combinations.

CURRENT DESIGN PHILOSOPHY

New design configurations generally evolve over a considerable length of time and involve aerodynamic analyses at the conceptual, preliminary, and detailed design levels, as shown in Figure 1. Therefore, analysis tools selected at each design stage must be compatible with the required accuracy and fit within the available budget. Normally, wind tunnel testing is integrated into the design process at the preliminary design stage to validate the aerodynamic predictions and contribute to configuration refinement. As better analytical tools are developed for application at each design stage, the amount of wind tunnel testing should decrease or one should, at least, be able to gain greater refinement while holding wind tunnel costs constant. There is a combination of analytical accuracy, cost, time required, and amount of wind tunnel testing that yields the best results at the lowest overall cost. Therefore, we must know which methods are most appropriate at any one time for any given application.

Design of multirole military aircraft requires evaluation of diversified flight regimes to determine optimum wing geometry. Consequently, the aircraft designers do not have the luxury of concentrating on a particular design point. To initiate a design study at General Dynamics, Fort Worth Division, a generalized conceptual design synthesis procedure (CDSP) (Reference 1) is used to determine the wing planform shape and size that best meets the multipoint design requirements. Gross effects of complex geometry characteristics, such as scheduled leading- and trailing-edge flaps, are included in the methodology. Once the planform is selected, linear theory, combined with empirical adjustments, is used to conduct a parametric study of camber and twist (or center of pressure for supersonic optimum camber) at selected design points. Effects of scheduled leading- and trailing-edge flaps are included and aeroelastic effects can be accounted for, if desired. A target drag level is established as a measure of merit at each design point. A plot, such as that shown in Figure 2, is constructed to show which camber designs meet or exceed the target drag levels. Attention is also given to pressure distribution characteristics. At this point, one or more candidate designs are selected for further detailed study. Refinement may consist of CFD code analyses as well as wind tunnel tests. Parametric variations are often accomplished at this stage but are restricted to a well defined "design space." As the design becomes more refined, the analysis codes used should become progressively more accurate.

Drag calculation is a central issue in the design philosophy. Although target pressures are often used in the wing optimization process, the drag level produced is the final measure of success. Therefore, the discussion of codes in this paper includes test-to-theory comparisons of drag as well as pressures. Multiple design point requirements and complex geometries of

fighter aircraft necessitate continued acquisition of parametric wind tunnel data. For example, General Dynamics has recently conducted a series of planform trades (Figure 3) that incorporate fully scheduled leading- and trailing-edge flaps that can be trimmed to high angles of attack. These data are also useful for CFD calibration as codes mature in the transonic regime. Before a code can be used with confidence, it is important to accomplish test-to-theory comparisons to assess its accuracy and to assure that the code is being used correctly. Some of the test-to-theory comparisons that have been accomplished at General Dynamics are presented in this paper. An overview of the codes for which comparisons are shown is presented below and is followed by the test-to-theory results.

AN OVERVIEW OF METHODS

Figure 4 summarizes several codes that are presently used to solve various forms of the flow equations; flow field characteristics handled by the codes are also shown. Results from several of the codes (shaded area in Figure 4) have been selected as representative of test-to-theory comparisons of fighter-type configurations. The codes selected are the US8 modified-linear theory code (Reference 2), WBPPW small disturbance code (Reference 3), TWING and TAWFIVE full-potential codes (References 4 and 5, respectively), and PARC2D and PARC3D Euler/Navier-Stokes codes (Reference 6).

Modified-Linear Theory

The US8 wing design code, developed at General Dynamics Fort Worth Division, is used for parametric wing design studies. The code employs an aerodynamic load matrix generated by the Carmichael panel method (Reference 7). In the Carmichael code, an arbitrary configuration is represented by up to 500 distributed singularities that satisfy the linearized potential equation. Experience has shown that better results are generally obtained for fighter-type configurations by representing both the body and lifting surfaces as wing-type members. Pressure loads are computed in US8 using the aerodynamic matrix in combination with configuration geometry (planform description and mean-line slopes). Lift, drag, and pitching moment characteristics are developed from these pressure loads. Calculation of the drag polar depends upon first determining the lower and upper bounds of drag. The upper bound of drag corresponds to the condition of zero leading-edge suction and is determined by integrating the products of the local pressure loads and local mean-line slopes. The lower bound of drag corresponds to 100 percent leading-edge suction and is calculated with the Sivells-Neely method (Reference 8) as a function of the span-load distribution. The actual predicted polar is determined using an empirically derived value of partial leading-edge suction, which positions the polar relative to the upper and lower bounds of drag. The polar break is also predicted by monitoring the leading-edge pressure values, and the drag polar above this break is degraded because of leading-edge suction loss.

Transonic Small Disturbance

WBPPW (Wing-Body-Pod-Pylon-Winglet) is used to solve a modified form of the small-disturbance equation by incorporating higher order terms to improve swept shock resolution and to provide improved approximation to the full potential equation at the critical velocity where the equation changes type

(elliptic to hyperbolic). The equation is solved in non-conservative form using an implicit finite-difference scheme. The code uses an internally developed rectangular Cartesian grid system. The configuration is placed within a crude grid with boundaries representing infinity and the symmetry plane. Fine grids are placed around each component; on these grids the detailed computations are performed. The crude grid provides a communication link between the individual fine grids. Viscous effects, including calculation of skin friction drag, can be included for lifting surfaces by using an option that couples a modified-Bradshaw boundary-layer technique (Reference 9) with the basic finite-difference scheme.

Full Potential

The TWING code (Transonic WING) solves the transonic full-potential equation in conservation form for an isolated wing on a wall. TWING utilizes a fully implicit, approximate-factorization algorithm. Since the code is written for an isolated wing, a two-dimensional grid-generation scheme is used at each span station with linear interpolation used to extend the grid to three dimensions. Wing geometry is input by the specification of breakpoint locations that define changes in leading-edge sweep, trailing-edge sweep, twist angle, inboard and outboard edges of part-span flaps, and flap deflections. Viscous effects are not included in the code.

TAWFIVE (Transonic Analysis of a Wing and Fuselage with Interacted Viscous Effects) solves the full potential equation using a conservative, implicit, finite-volume technique. The program is a combination of the Caughey-Jameson FLO-30 code (Reference 10) and a fully three-dimensional, compressible, boundary-layer method (References 11 and 12). An internal grid generator produces a Joukowsky-parabolic conformally mapped grid for a wing-body configuration. This grid is best suited for wings of moderate sweep, aspect ratio, and taper ratio (transport-type wings). The geometry input consists of a series of airfoil sections to define the wing and a series of fuselage sections to define an arbitrary fuselage.

Euler and Navier-Stokes

PARC2D and PARC3D solve the complete Navier-Stokes equations in conservative form using the Beam and Warming approximate factorization algorithm. In addition to solving the complete Navier-Stokes equations, the viscous terms can be selectively included so that either a thin-layer simulation can be performed or an inviscid (Euler) flow field can be calculated. For viscous simulations, turbulent flow is calculated by using Reynolds averaging and by employing an algebraic turbulence model. The algorithm is formulated for a curvilinear set of coordinates; therefore, quite complex geometries can be analyzed.

TEST-TO-THEORY COMPARISONS

For test-to-theory discussions, the codes are divided into three classes: (1) linear theory and modified-linear theory, (2) small disturbance and full potential, and (3) Euler and Navier-Stokes. A few of the validation activities that are under way in the transonic flow regime are discussed in subsequent paragraphs.

Linear theory has well-known limitations and at first seems to be inappropriate for transonic application. However, when drags are calibrated with experimental results on similar configurations and pressure levels are monitored for separation based on previous experience, linear theory can become a powerful design tool for military multirole aircraft application. Design visibility for camber and twist can rapidly be obtained for multiple design conditions, e.g., cruise, transonic maneuver, acceleration, and often includes the important effects of scheduled leading- and trailing-edge flaps and trim. This process would be time-consuming using the second-level codes and an impossible task employing third level codes with today's hardware.

Second-level codes fit in the design process (Figure 1) very nicely as the next step after linear theory has been used. Optimization is still practical with these codes, but our approach is to use them as a refinement to the initial linear theory design.

Because of the time required to generate grids and solutions and considering computer costs, third level codes are generally used to address specific design problems and are employed as final refinements for particular geometry and flow condition combinations.

Test-to-theory comparisons were accomplished for the planform in Figure 5 with and without camber and flaps to assess how well each code predicts camber and flap effects, a key part of a wing design process. Lift, drag, and moment calculations for the uncambered wing are compared with test data in Figure 6 at Mach 0.9. The modified-linear theory actually shows the best overall correlation, although the drag levels have been calibrated with test data from a similar configuration. TWING results are somewhat better than those from TAWFIVE and WBPPW. Furthermore, converged solutions were obtained to a higher angle of attack for TWING than for TAWFIVE or WBPPW. TWING's success at the higher angles of attack can, in part, be attributed to an option in the code that allows for an approximation of a rotated differencing scheme in regions of local supersonic flow.

For this planform, the TAWFIVE code experienced difficulties in convergence at grid points near the tip. As revealed in Figure 7, the internally generated grid produced very sharp angles in the spanwise grid lines as the lines extend off the tip of the wing. This situation was circumvented by generation of an external grid. As shown in Figure 8, the spanwise grid lines are much smoother as the lines extend off the tip. A realistic representation of the fuselage was also incorporated in the grid system.

The ability to accurately predict drag and pitching moment increments attributed to camber is an important factor in the selection of a code used in the design environment. Comparisons shown in Figure 9 reveal that all the codes predict increments that compare reasonably well with the experimental data.

For a wing design code to be useful in fighter aircraft design, the code should accurately predict flap effects or at least indicate that calibration factors be developed to allow flap effects to be predicted with confidence. Incremental flap effects at 0.9 Mach number are compared with experimental results in Figures 10 and 11. Drag and moment trends are predicted quite well

with both linear theory and TWING for leading- and trailing-edge flap deflections of 10 degrees. TWING yields better drag increment predictions but linear theory provides somewhat better correlation of moments. Both over-predict the trailing-edge flap moment effect, which is common and can be accounted for with suitable calibration factors. Both codes provide comparable results for forces and moments. Of course, TWING has the advantage of providing more realistic simulation of the transonic flow field because of its ability to predict shocks.

Additional insight into the transonic codes is revealed in test-to-theory comparisons obtained for the F-16 configuration (Figure 12). The configuration was analyzed with wing-alone geometry in TWING and WBPPW while the simulation used in TAWFIVE consisted of the wing mounted on a semi-infinite axisymmetric cylinder. Symmetrical NACA 64A airfoils were employed between the centerline and Span Station 53.0 (the region of the theoretical planform covered by the strake and fuselage) in the TWING and WBPPW simulations. Typical force and moment plots obtained from these codes at Mach 0.9 are presented in Figure 13. Lift and drag were predicted reasonably well by all codes. Specifically, WBPPW and TAWFIVE predicted lift well but tended to predict higher drag levels. Drag was predicted very well by TWING for lift coefficients below 0.6. Good correlation of lift was obtained for angles of attack between 2 and 7 degrees. For angles of attack greater than 7 degrees, the experimental lift curve becomes dominated by flow separation and vortex lift. A variation between the codes was evident in the prediction of moments. Although TAWFIVE did a good job of predicting C_{M_O}, the predicted aerodynamic center is too far forward. In contrast, WBPPW does a better job of predicting the a.c., but misses the C_{M_O}. TWING predicts C_{M_O} reasonably well and the a.c. is very close to the test data below a lift coefficient of 0.5.

Pressure distributions for 4.1 degrees angle of attack are presented in Figure 14. The experimental pressures at the first span station ($\eta = 0.32$) show considerable influence of the strake since this station is only four inches outboard of the wing/strake intersection. Local flow separation produced by the vortical flow results in the lack of a leading-edge pressure peak. Experimental data show a leading-edge pressure peak at all other span stations, and TWING predicts the peak pressures better than TAWFIVE. WBPPW does not predict a leading-edge pressure peak. The inability of TAWFIVE and WBPPW to adequately predict the leading-edge pressures results in a lower loading on the leading edge of the airfoil. This lower loading contributes to a more nose-down pitching moment inboard of $\eta = 0.59$. Outboard of this station, a more nose-up moment results from this lower loading. Over the plateau region of the pressure distributions (10- to 63-percent chord), all three codes compare reasonably well with both upper and lower surface experimental data. However, the inclusion of viscous effects would shift all of the upper surface curves down, thereby improving the TWING comparisons (except at the tip station). These plots also reveal that TWING consistently predicts the trailing-edge shock location better than either TAWFIVE or WBPPW.

Correlation of TWING predictions with test data is shown in Figure 15 for the F-16 wing with leading-edge flap deflections of 0, 5, and 10 degrees. Corresponding pressure comparisons are shown in Figure 16 at 6.06-degree angle of attack for 5-degree leading-edge flap deflection. Force and pressure comparisons again show that TWING predicts lift values and pressure levels

that agree reasonably well with experimental data in regions where viscous effects are not significant. Over-prediction of shock strength, exhibited in Figure 16, lends support to the rule of thumb suggested by Cosentino and Holst (Reference 13) that shock strengths are over predicted when the local Mach number ahead of the shock is greater than 1.3. Examination of the predicted pressures throughout the range where convergence was obtained with TWING indicates that, for local Mach numbers less than 1.2, shock strengths agreed quite well with experiment. Above Mach 1.3, the predicted shock waves were always too strong. For local Mach numbers between 1.2 and 1.3, shock wave agreement was not consistent.

F-16 results, presented here and those shown earlier for the generic wing-body, suggest that TWING generally provides better results for thin-wing, low-aspect ratio fighters than the other methods shown. Therefore, we decided to compare results to those obtained from an Euler code. The PARC Euler code was selected because of its present widespread industry usage. An F-16 wing-alone simulation was used in PARC to duplicate the geometry used in TWING. Comparisons of lift, moment, and drag are shown in Figure 17. PARC solutions were obtained only at 0-, 2-, and 4.1-degrees angle of attack. For these conditions, PARC and TWING produce comparable results, both of which are very good. Pressure data are compared in Figure 18 at 4.1-degrees angle of attack. Again, the comparisons with test data are in general quite good. TWING does a better job of predicting the leading-edge pressure peak while PARC is better at predicting the shock strength. The codes provide comparable results for shock location.

PARC2D was used to analyze an axisymmetric nozzle at Mach 1.2. A Navier-Stokes solution was obtained using the Beam and Warming implicit solution algorithm and a Baldwin-Lomax turbulence model. The analysis required approximately one CPU hour of CRAY X-MP/24 time. A comparison of predicted and test outer surface pressures is shown in Figure 19. Test and predicted values of drag and thrust are also shown. Both the pressures and forces correlate very well with the experiment.

General Dynamics has an ongoing cooperative effort with NASA Ames and the Air Force Flight Dynamics Laboratory to validate CFD codes through use of the extensive F-16 data base. As part of this effort an Euler analysis of the complete F-16 has been accomplished. Preliminary results were presented at a 1986 AGARD Symposium (Reference 14). Part of the grid system, which has over 500,000 grid points in 20 blocks, is shown in Figure 20. Detailed modeling of the inlet and nozzle with flow-through boundary conditions is essential for full aircraft simulation with power effects. Details of the inlet grid blocking are shown in Figure 21.

Calculations, which were made on the Fort Worth Division CRAY X-MP/24 and the NASA Ames CRAY 2, employed approximately thirty-five CPU hours. Computed velocity vectors on the surface of the forward fuselage are shown in Figure 22. Accuracy of the fuselage flow field calculations was further verified by an excellent comparison between computational results and experimental pressure coefficients from Reference 15. Sample comparisons at two fuselage stations are shown in Figure 22.

Since this was the first time that an analysis of this magnitude had been attempted, it was no surprise that problems were encountered. The code simply did not develop shock waves at the downstream edge of the supersonic bubble on the wing upper surface; consequently, pressures in this region were not accurately predicted. To address the problem, a denser grid system is being incorporated on the wing upper surface that will provide for better shock resolution. In addition, the code has been recently modified to allow for full Navier-Stokes solutions. Further computations are planned on the NASA/Ames Numerical Aerodynamics Simulator.

THE FUTURE OF APPLIED CFD

CFD capability is rapidly maturing and is now routinely used in the design process. Applications of first and second level codes have progressed to complex configurations at transonic speeds, but solutions of the more rigorous level three (Euler and Navier-Stokes) flow equations are time consuming and only practical for detailed design. With continued improvement in grid generation concepts and algorithms and the natural evolution in computer hardware, we can look forward to routine application in the preliminary design phase for complex geometries at increasingly more complex flow conditions. In the meantime, the applied aerodynamicist must rely on the faster codes for the important optimization tasks. We have advanced from total reliance on linear theory to more and more use of small-disturbance and full-potential codes. We must continue to improve the adaption of these intermediate level methods to aircraft design for optimization.

Code validation remains a major task, particularly for the more sophisticated codes applied to complex geometries. Studies to verify grid independence and to determine regions of applicability (Mach, angle of attack, Reynolds number, etc.) are expensive and time consuming but indispensable to achieve credibility.

Comparisons with experimental data must include forces and moments in addition to the common comparisons with flow fields and pressure dis-distributions. We must work toward more quantifiable validation. Color pictures of flow fields are impressive but, by themselves, do not provide sufficient credibility for the design engineer.

For fighter applications, one of the most fruitful and most difficult areas for CFD application is at high angles of attack including the transonic regime. Current design practice requires significant wind tunnel refinement to achieve desired lateral/directional and longitudinal stability characteristics. These flows are heavily influenced by strong forebody vortex interaction with strakes, wings, and control surfaces. Accurate consideration of viscous effects (turbulence modeling), vortical flow and, most likely, dynamics are required in addition to complete 3-D geometry modeling. The capability to accurately model this flow regime will provide the design engineer with a good barometer of the CFD developer's progress.

Additional emphasis must be placed on the capability to predict drag accurately, for this will always be the performance bottom line. We must progress beyond the pressure monitoring approach, particularly in the

transonic regime, which is critical for cruise and maneuver design. The fidelity that comes with accurate drag predictions is required before CFD will reach its full potential as a design tool.

REFERENCES

1. A. G. Chavera, "The Conceptual Design Synthesis Program (CSDP)," General Dynamics Report FZA-552, 1 February 1986.

2. W. W. Braymen and C. Q. Pass, "Aerodynamic Wing Design and Analysis Methods," General Dynamics Report ERR-FW-2397, December 1983.

3. C. W. Boppe, "Transonic Flow Field Analysis for Wing-Fuselage Configurations," NASA CR-3243, May 1980.

4. G. B. Cosentino and T. L. Holst, "Numerical Optimization Design of Advanced Transonic Wing Configurations," NASA TM 85950, May 1984.

5. N. D. Melson and C. L. Streett, "TAWFIVE: A User's Guide," NASA TM 84619, September 1983.

6. G. K. Cooper, "The PARC Code: Theory and Usage," AEDC-TR-87-24, October 1987.

7. R. L. Carmichael, C. R. Castellano, and F. C. Chen, "The Use of Finite-Element Methods for Predicting the Aerodynamics of Wing-Body Combinations," Symposium on Analytical Methods in Aircraft Aerodynamics, Ames Research Center NASA SP-228, 28-30 October 1969.

8. J. C. Sivells and R. H. Neely, "Method of Calculating Wing Characteristics by Lifting-Line Theory Using Nonlinear Section Lift Data," NACA TN 1269, 1947.

9. P. Bradshaw and D. H. Ferriss, "Calculation of Boundary Layer Development Using the Turbulent Energy Equation. Compressible Flow on Adiabatic Walls," J. Fluid Mechanics, Vol. 46, 1971.

10. A. Jameson and D. A. Caughey, "A Finite-Volume Method for Transonic Potential Flow Calculations," Proceedings of AIAA 3rd Computational Fluid Dynamics Conference, June 1977.

11. P. D. Smith, "An Integral Prediction Method for Three-Dimensional Compressible Turbulent Boundary Layers," Royal Aeronautical Establishment R&M 3739, 1974.

12. H. W. Stock, "Integral Method for the Calculation of Three-Dimensional, Laminar and Turbulent Boundary Layers," NASA TM 75320, 1978.

13. G. B. Cosentino and T. L. Holst, "Numerical Optimization Design of Advanced Transonic Wing Configurations," NASA TM 85950, May 1984.

14. S. L. Karman, Jr., J. P. Steinbrenner, and K. M. Kisielewski, "Analysis of the F-16 Flow Field by a Block Grid Euler Approach," AGARD Paper No. 18, 58th Meeting of the Fluid Dynamics Panel Symposium, Aix En-Provence, France, April 1986.

15. G. H. Reue, M. E. Doberenz, and D. D. Wilkins, "Component Aerodynamic Loads From 1/9-Scale F-16A Loads Model," General Dynamics Report No. 16PR316, May 1976.

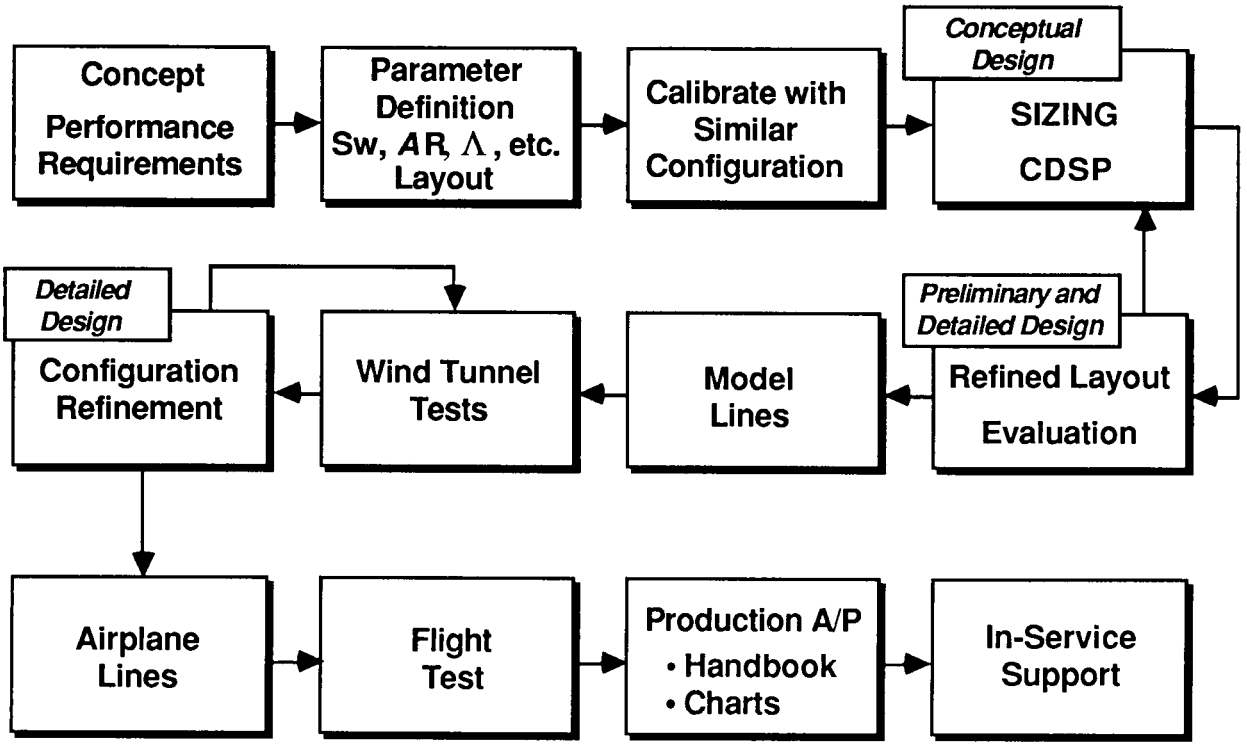

Figure 1. The Design Process

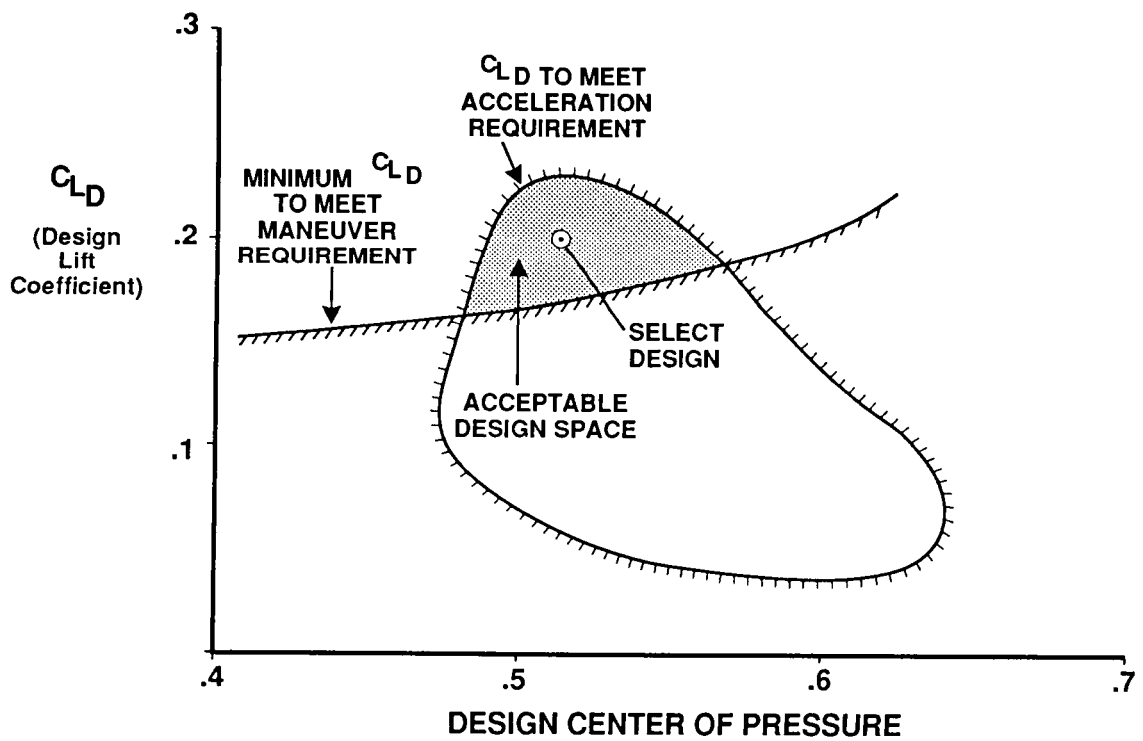

Figure 2. Illustration of Design Space

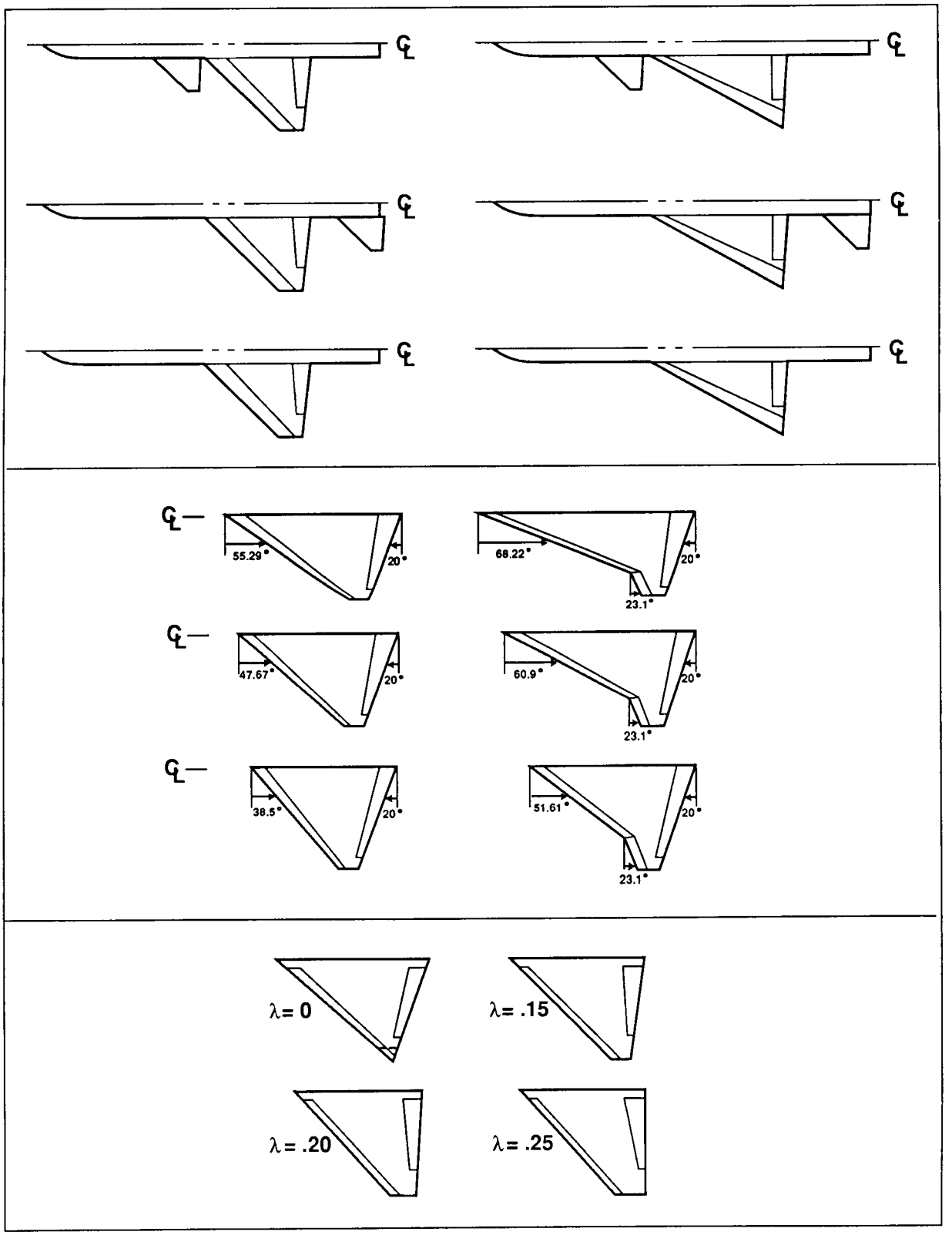

Figure 3. Parametric Models

EQUATION TYPE	EXAMPLE CODES	COMPRESSIBLE	NONLINEAR	UNSTEADY	ROTATIONAL	VISCOUS	HEAT TRANSFER
		CAPABILITIES					
• LINEAR VELOCITY POTENTIAL	WOODWARD, CARMICHAEL/US8 CUNNINGHAM, HESS, USSAERO, VSAERO, PAN AIR	✓					
• TRANSONIC SMALL DISTURBANCE	BAILEY/BALLHAUS, WBPPW, PANDORA, CANTATA	✓	✓				
• FULL POTENTIAL	FLO 22, FLO 27, FLO 28, FLO 30, TWING, TAWFIVE, GARABEDIAN/KORN (2-D)	✓	✓				
• EULER	FLO 57, FLO 58, SKOAL FALCON, PARC2D, PARC3D	✓	✓	✓	✓		
• NAVIER-STOKES	NS3D, ARC3D, PARC3D, FALCON, NS2D, ARC2D, PARC2D	✓	✓	✓	✓	✓	✓

Figure 4. Representative Codes

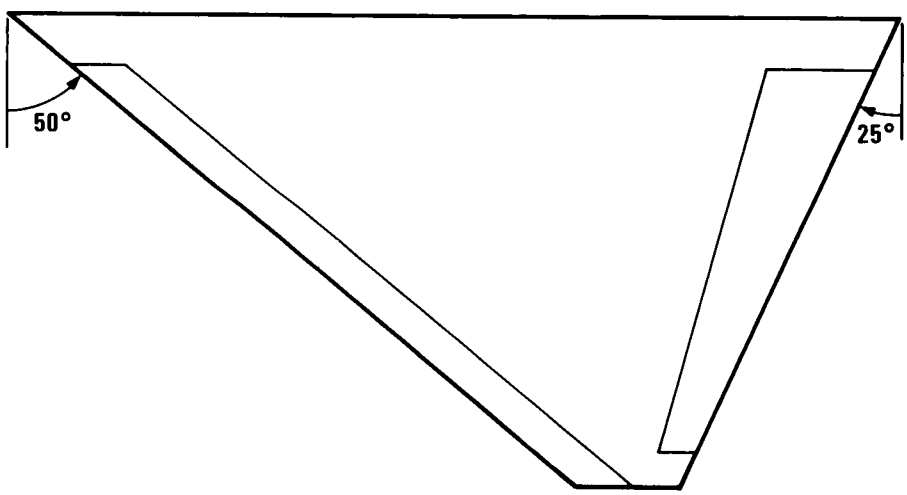

Figure 5. Selected Generic Planform

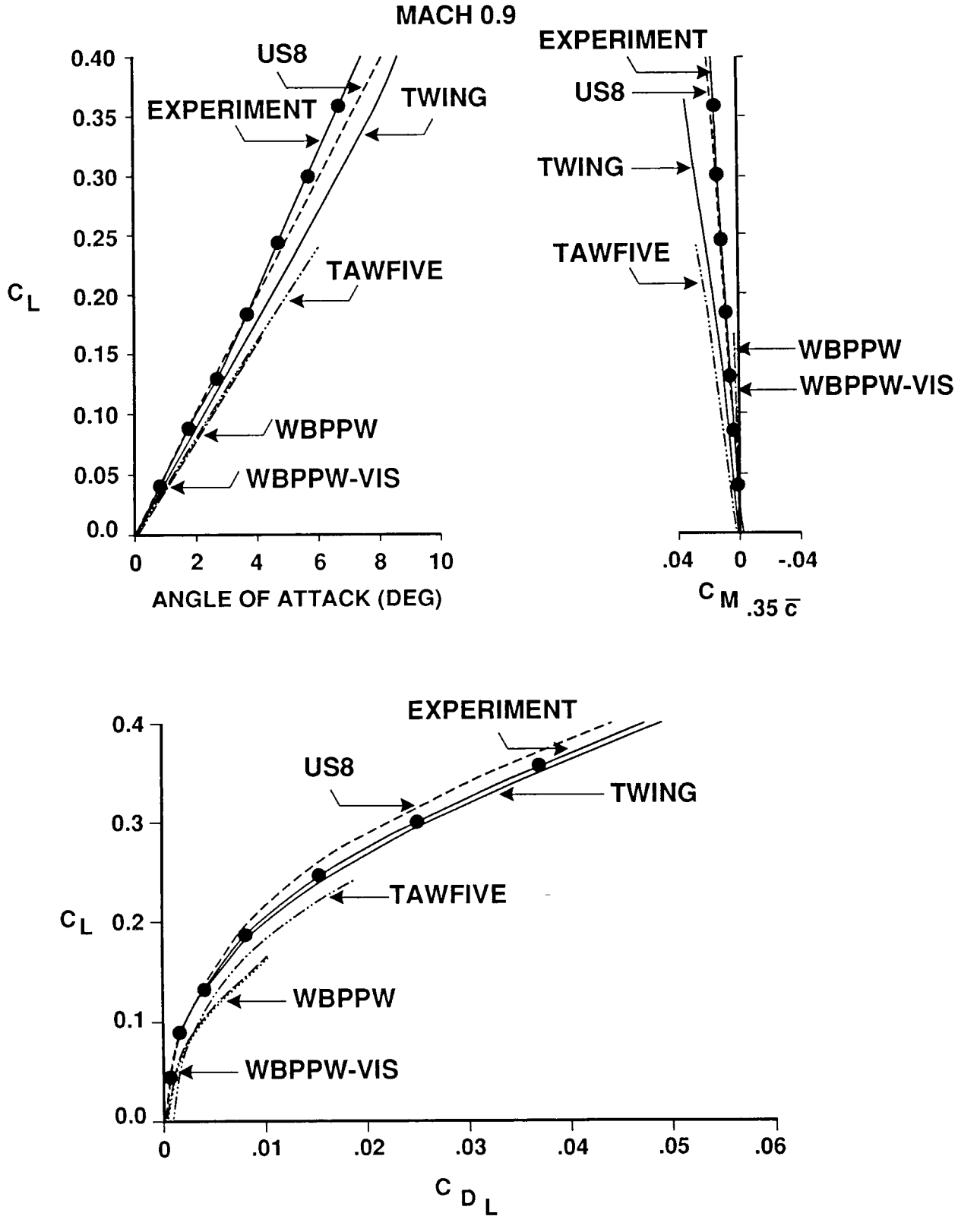

Figure 6. Test-to-Theory Comparisons of Uncambered Generic Wing at Mach 0.9

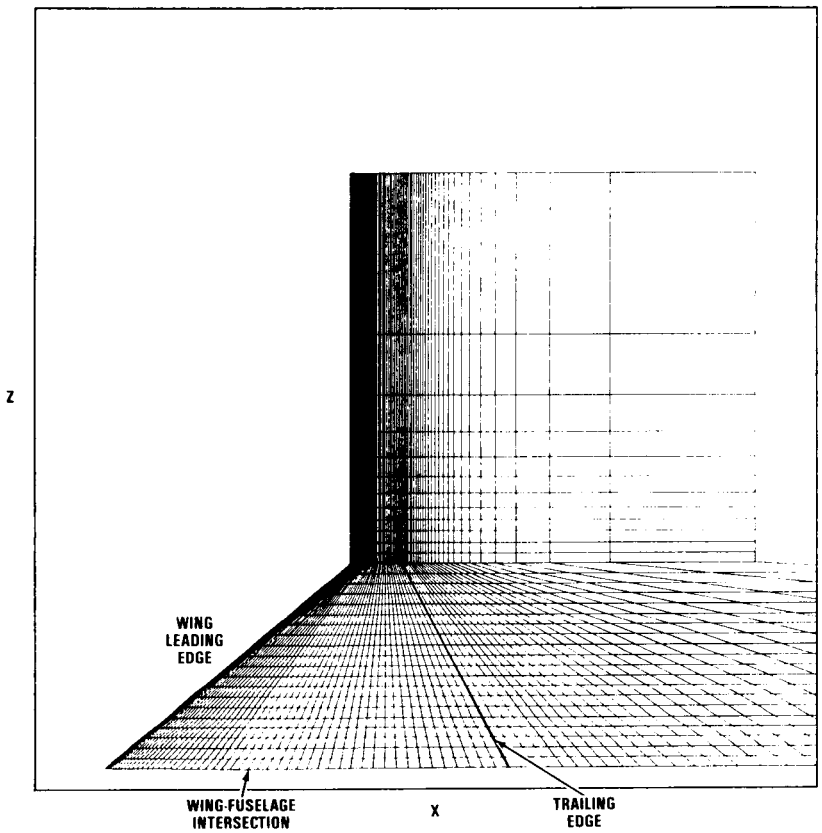

Figure 7. Generic Wing-Body Grid Generated Internally by TAWFIVE

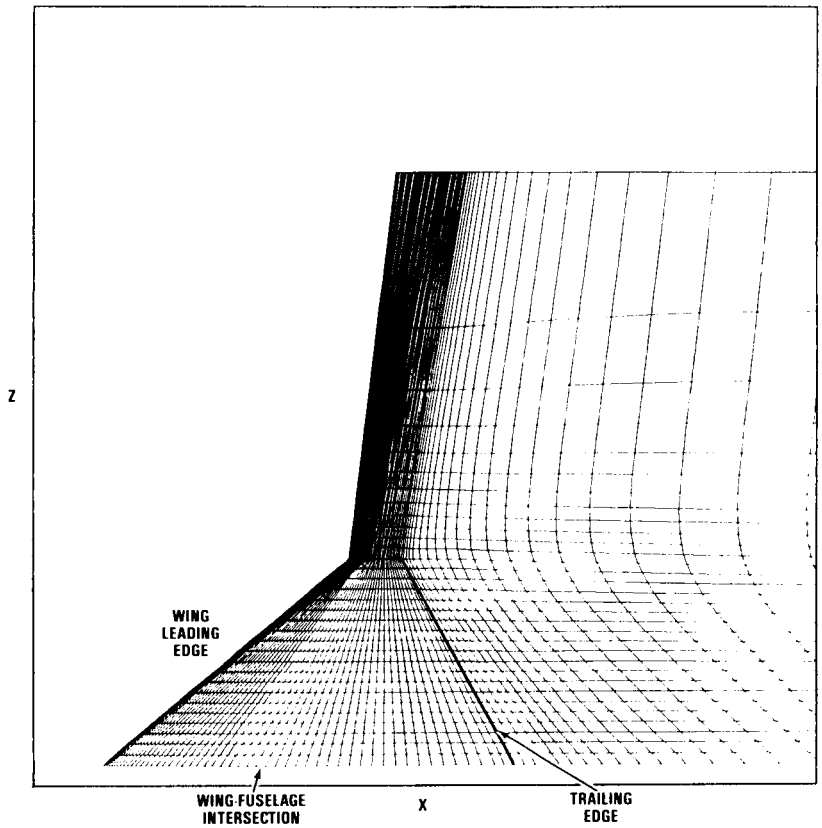

Figure 8. External Grid Used in TAWFIVE

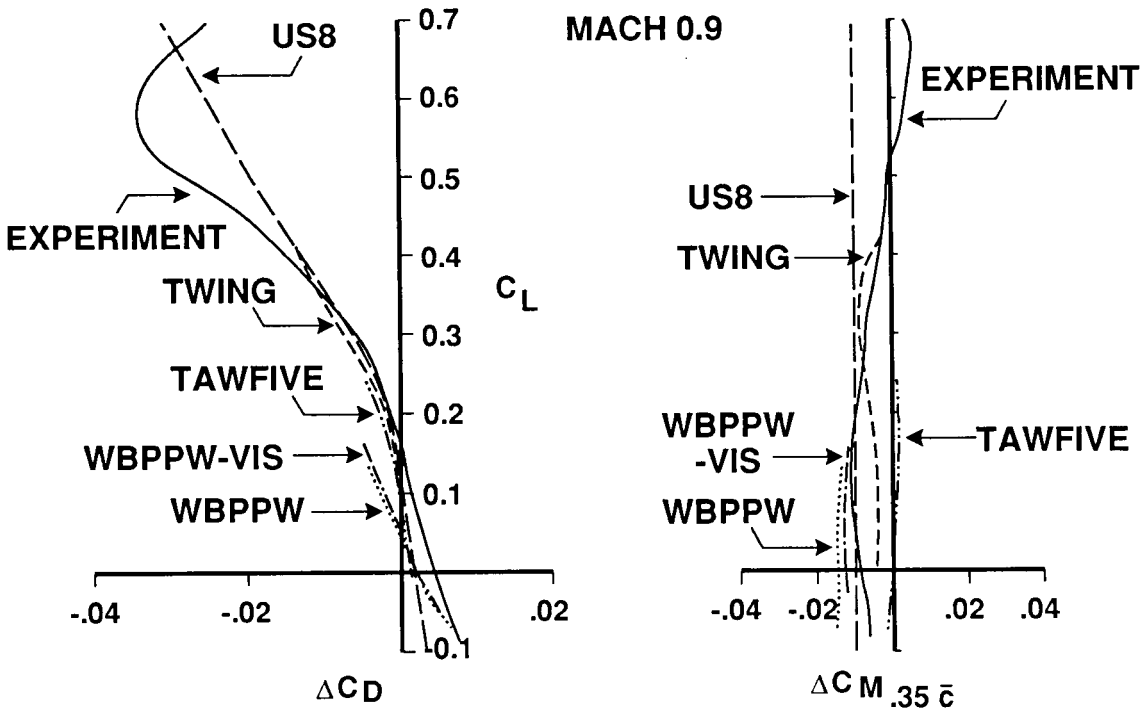

Figure 9. Camber Increment Comparisons

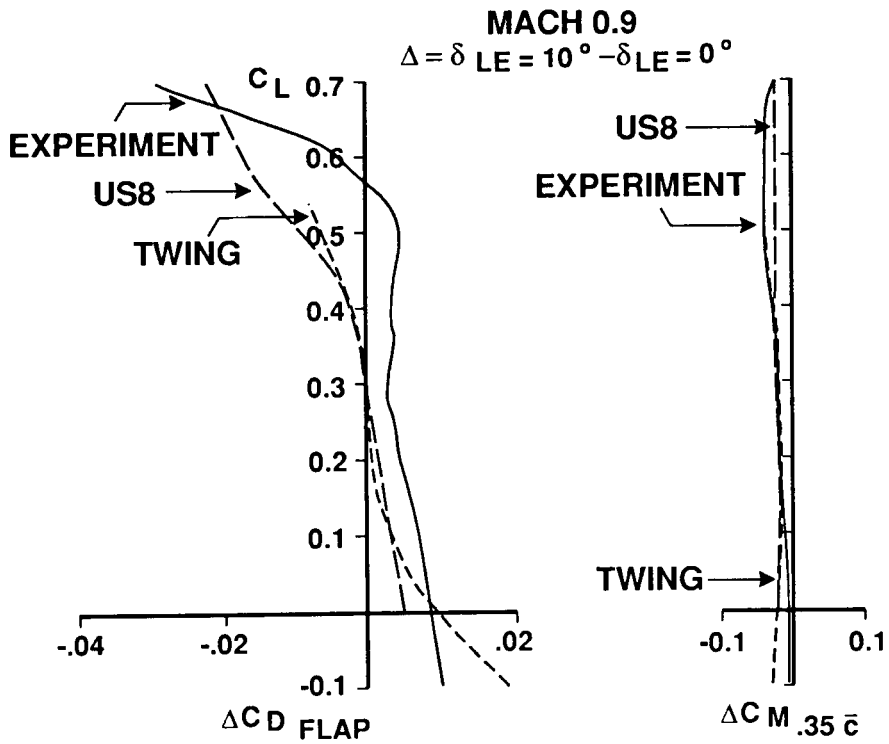

Figure 10. Comparison of Leading-Edge Flap Increments

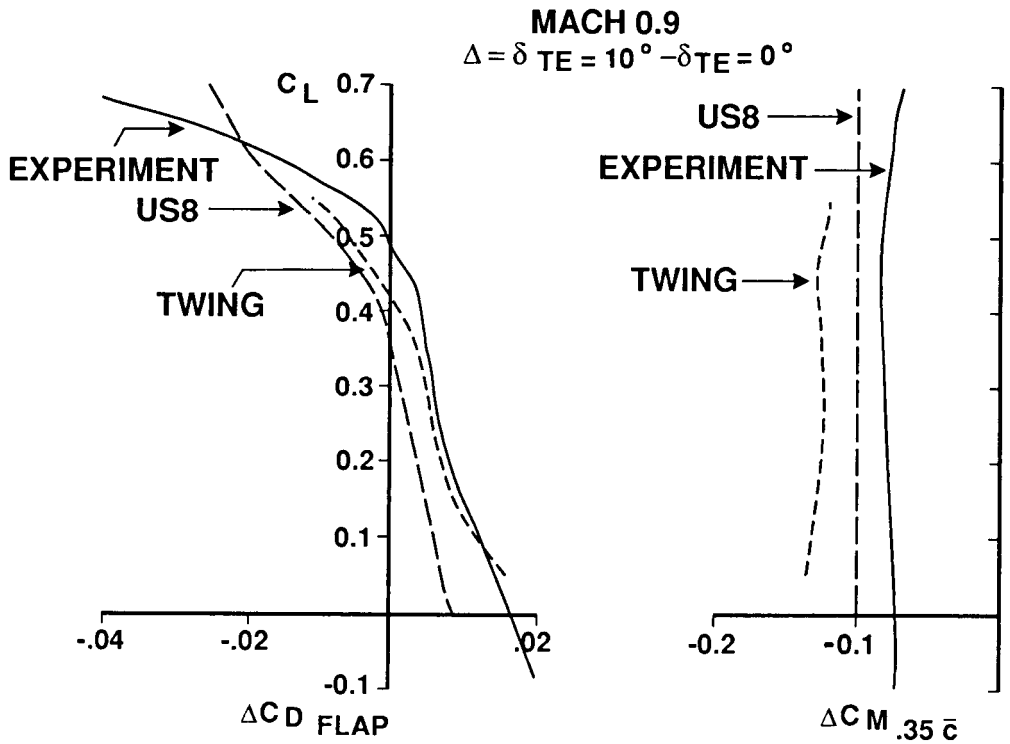

Figure 11. Comparison of Trailing-Edge Flap Increments

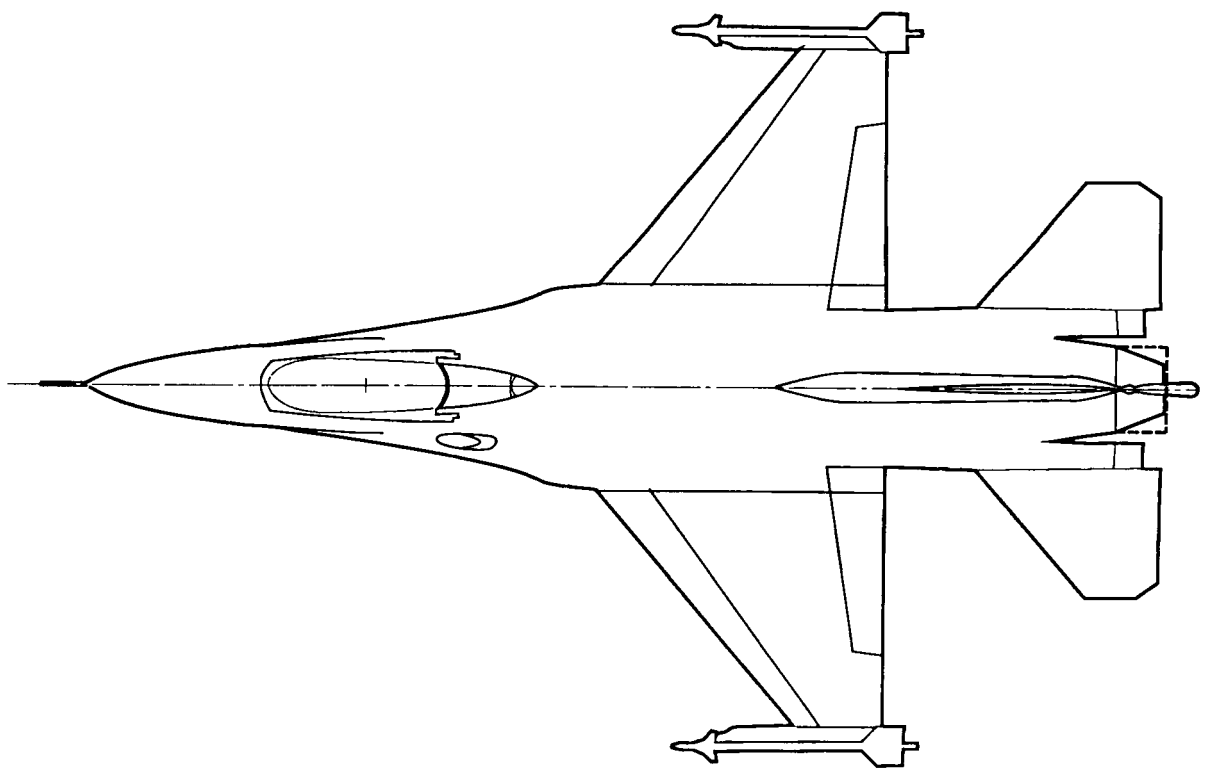

Figure 12. F-16 Configuration

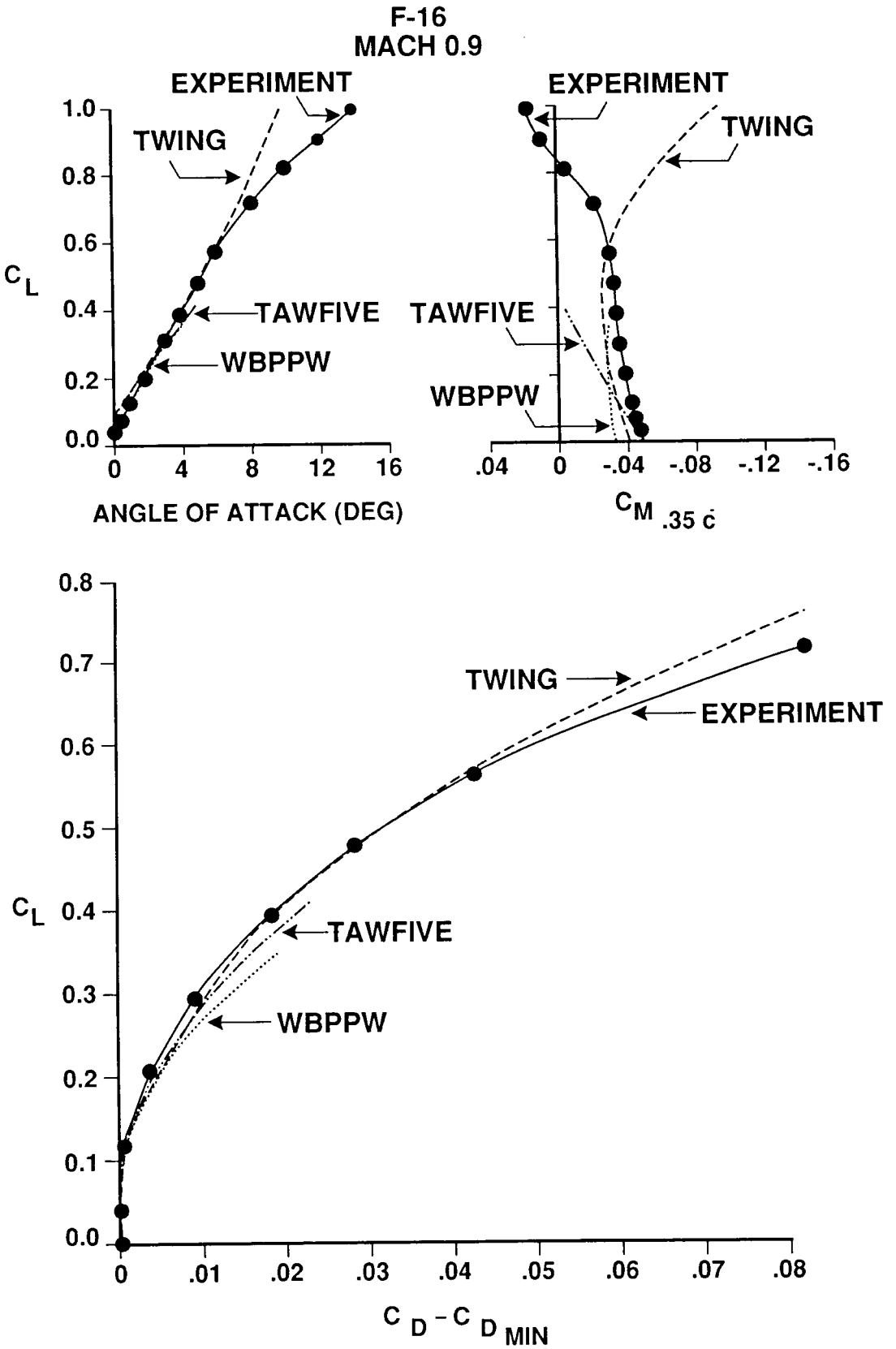

Figure 13. Test-to-Theory Comparison of F-16 Forces and Moments at Mach 0.9

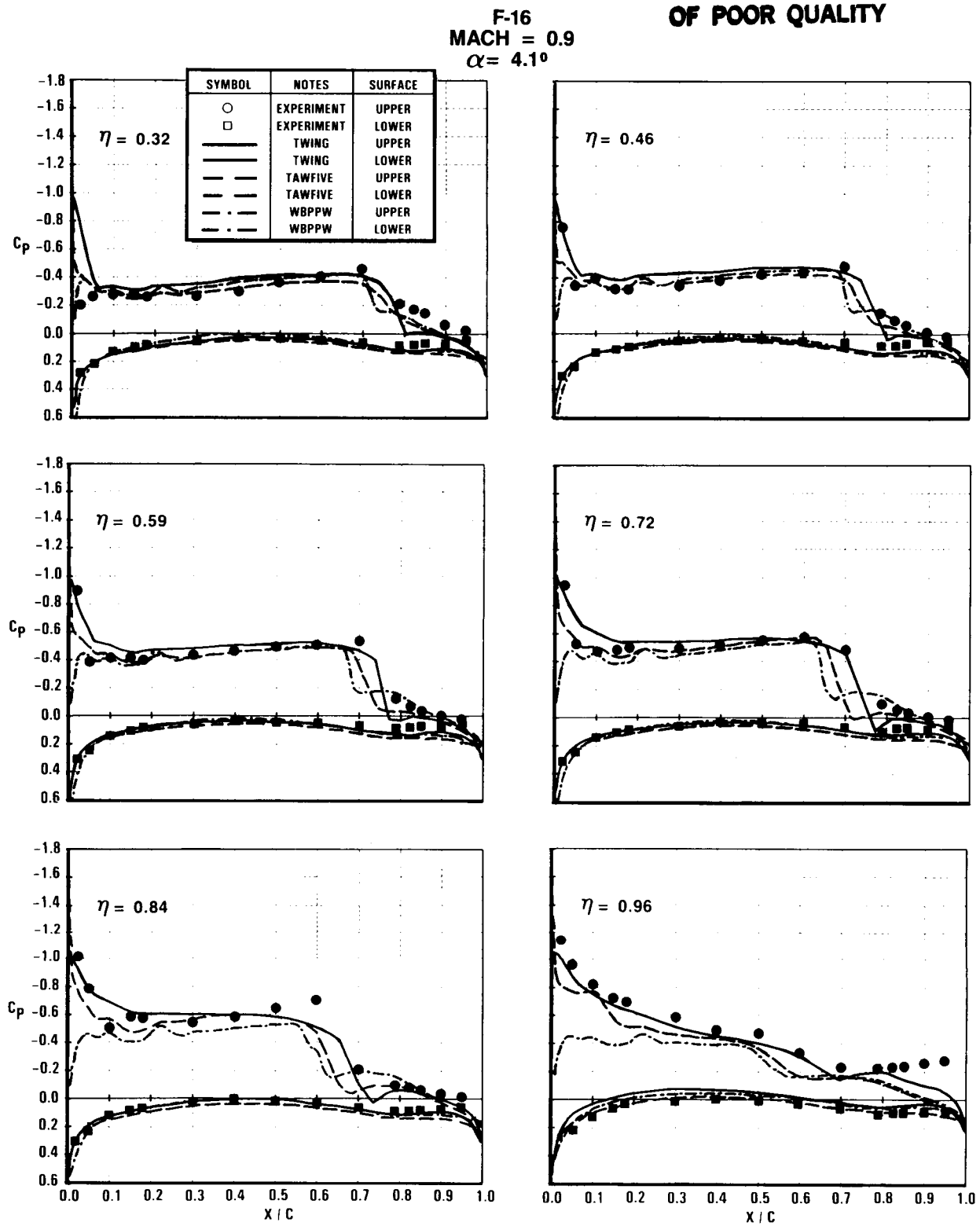

Figure 14. Comparison of F-16 Wing Pressures at Mach 0.9 and Angle of Attack of 4.1°

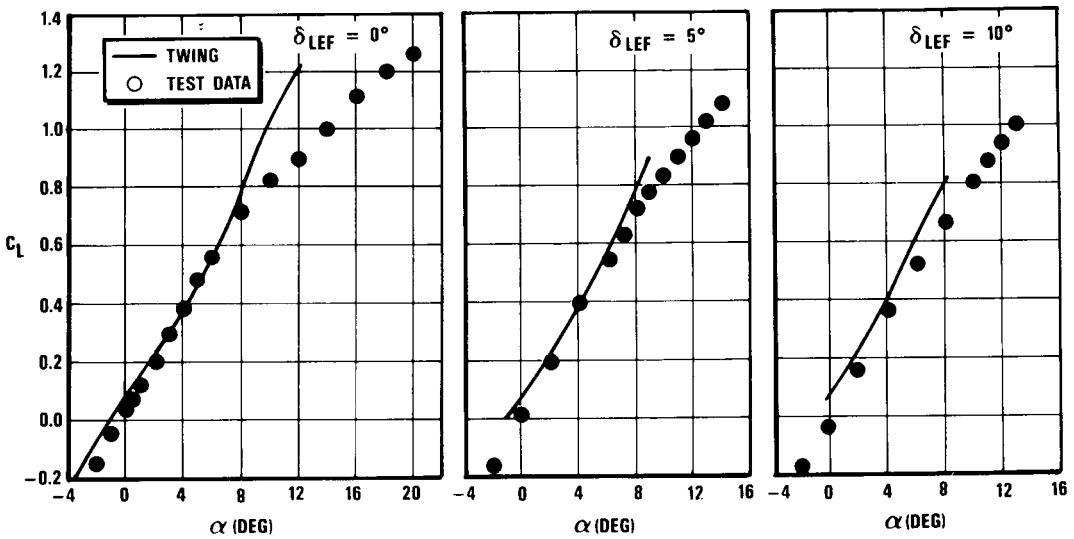

Figure 15. Comparison of F-16 Lift Curves at Mach 0.9 for Leading-Edge Flap Deflections of 0, 5, and 10 Degrees

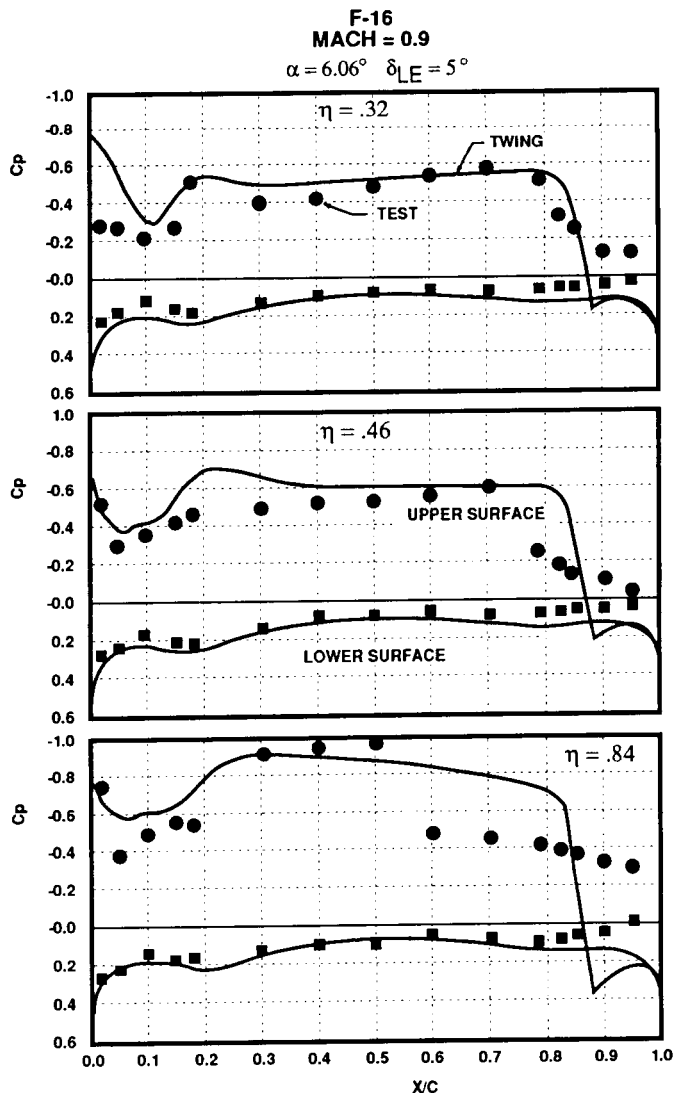

Figure 16. Comparison of F-16 Pressures with Deflected Leading Edge Flaps

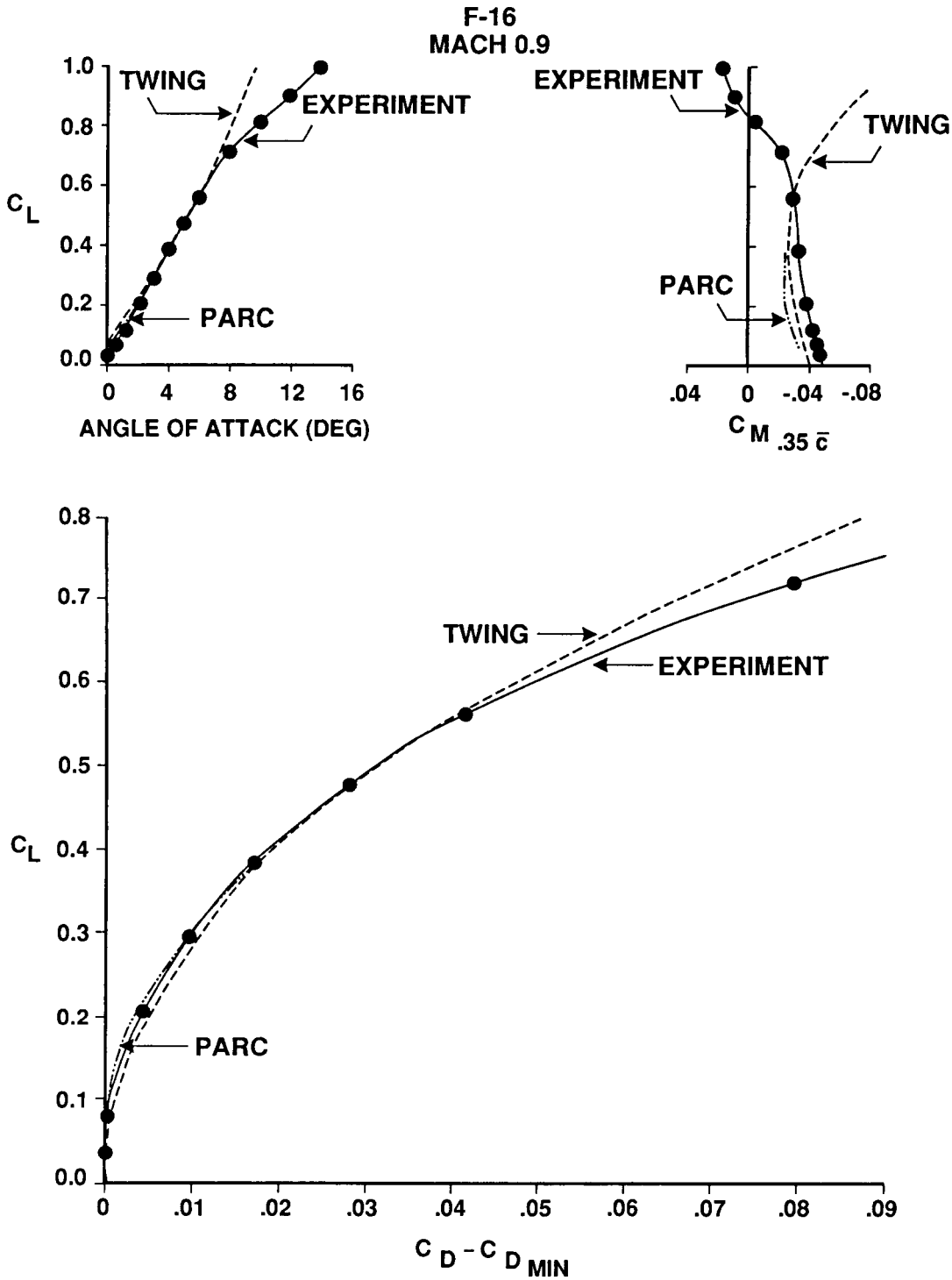

Figure 17. Comparison of PARC3D and TWING Force Predictions with F-16 Test Data at Mach 0.9

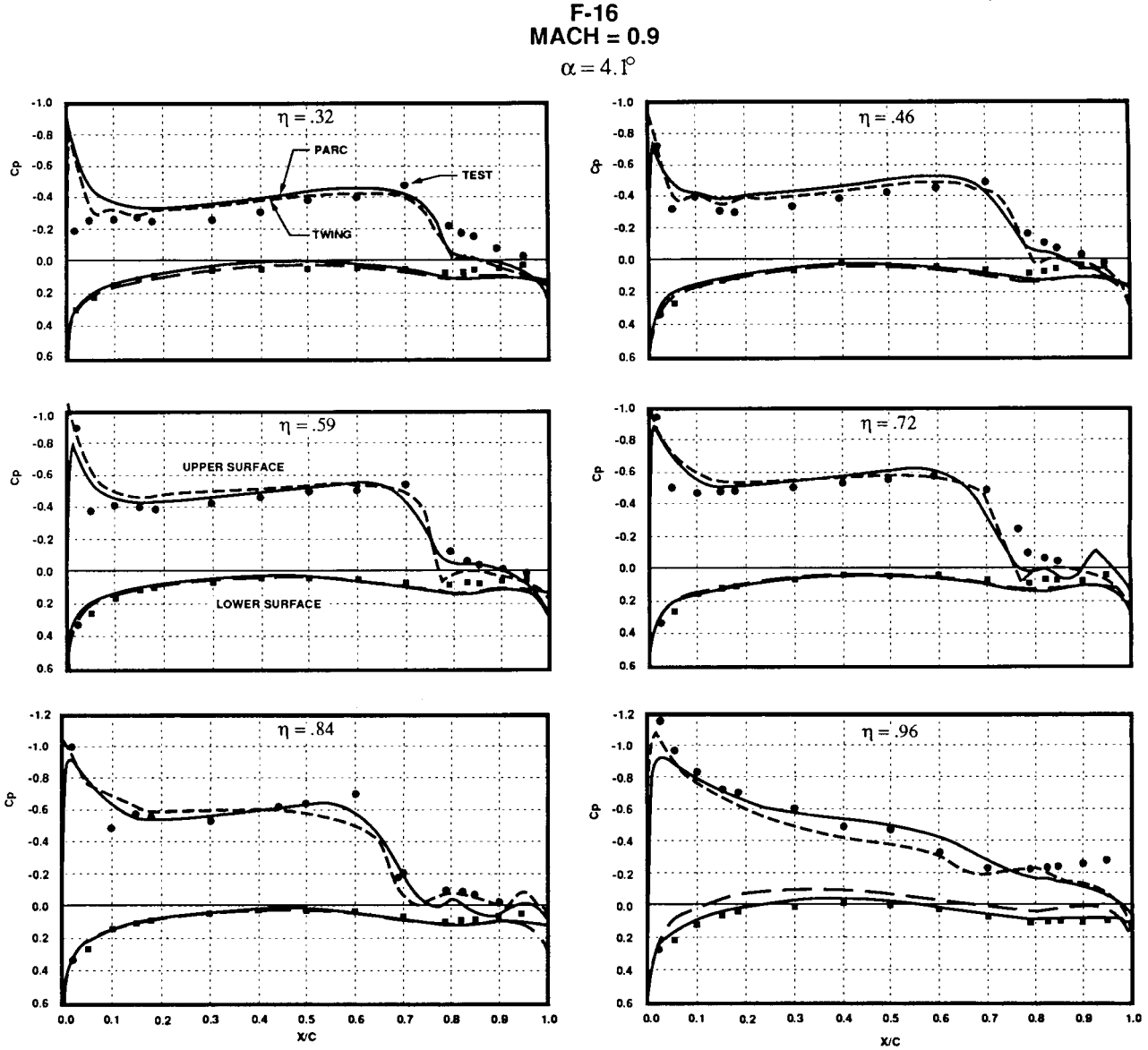

Figure 18. Comparison of PARC 3D and TWING Pressure Predictions with F-16 Test Data at Mach 0.9

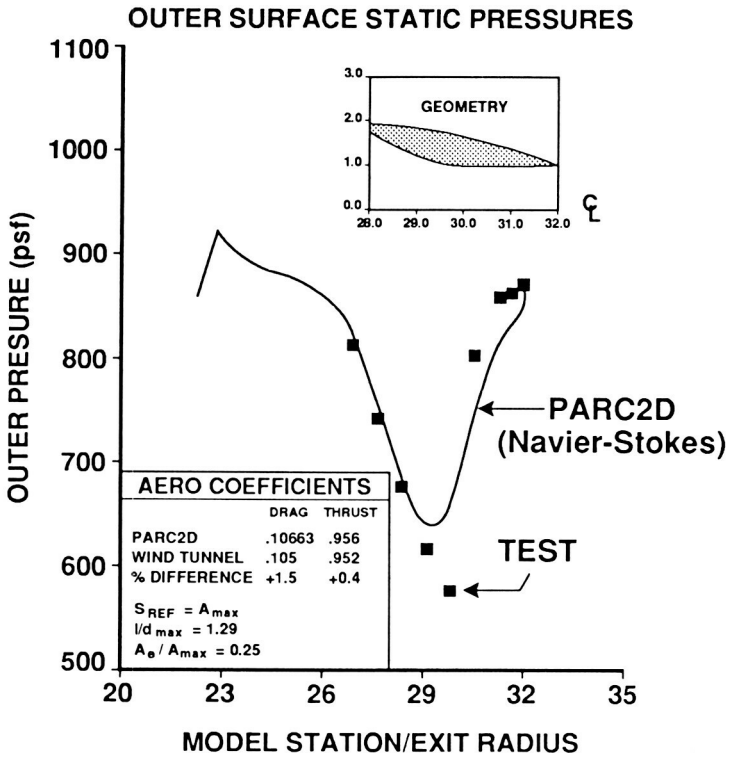

Figure 19. Test-to-Theory Comparison of Forces and Pressures on Axisymmetric Nozzle at Mach 1.2

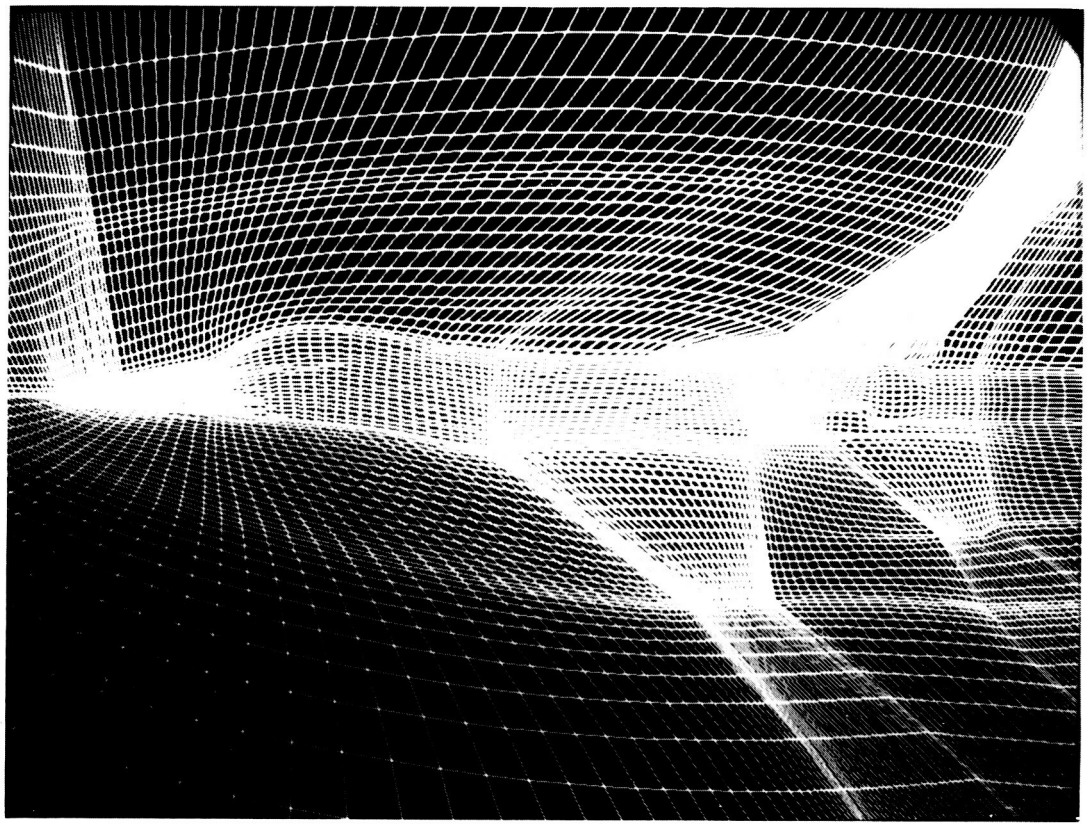

Figure 20. Grid System for Complete F-16 Representation

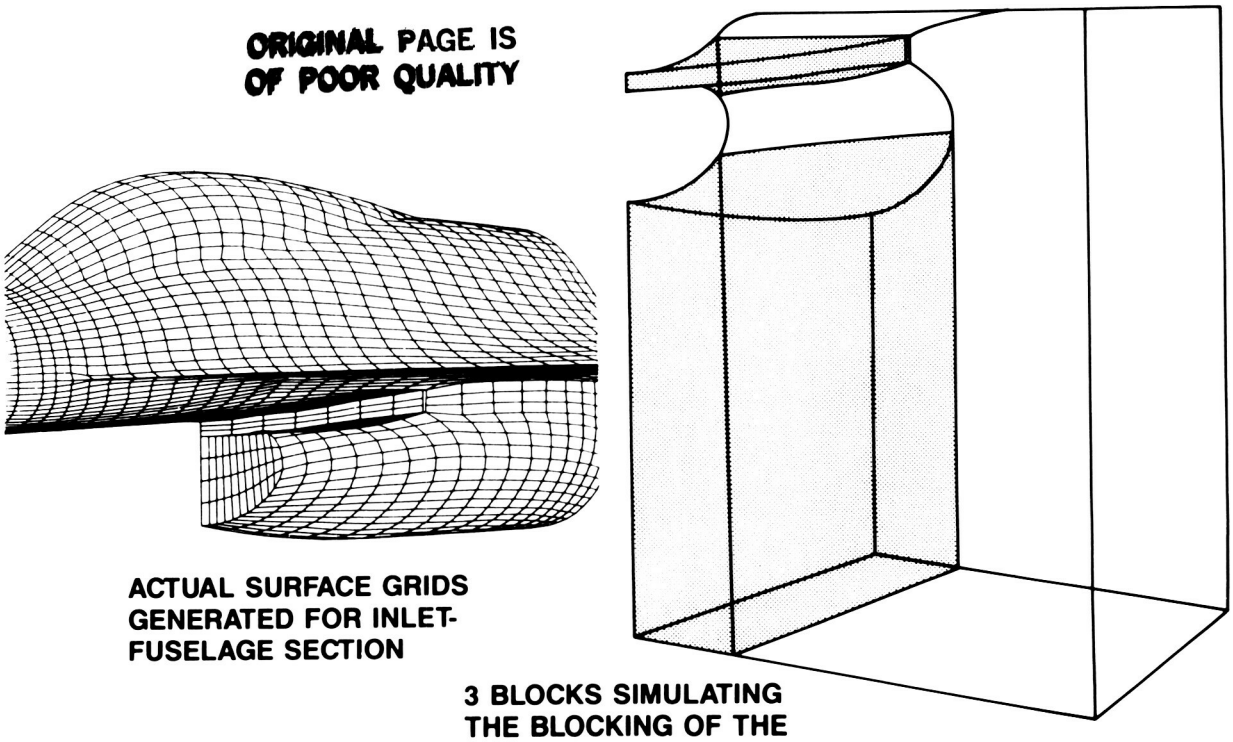

ACTUAL SURFACE GRIDS
GENERATED FOR INLET-
FUSELAGE SECTION

3 BLOCKS SIMULATING
THE BLOCKING OF THE
INLET-FUSELAGE REGION

Figure 21. Blocking Scheme Applied to F-16 Inlet Region

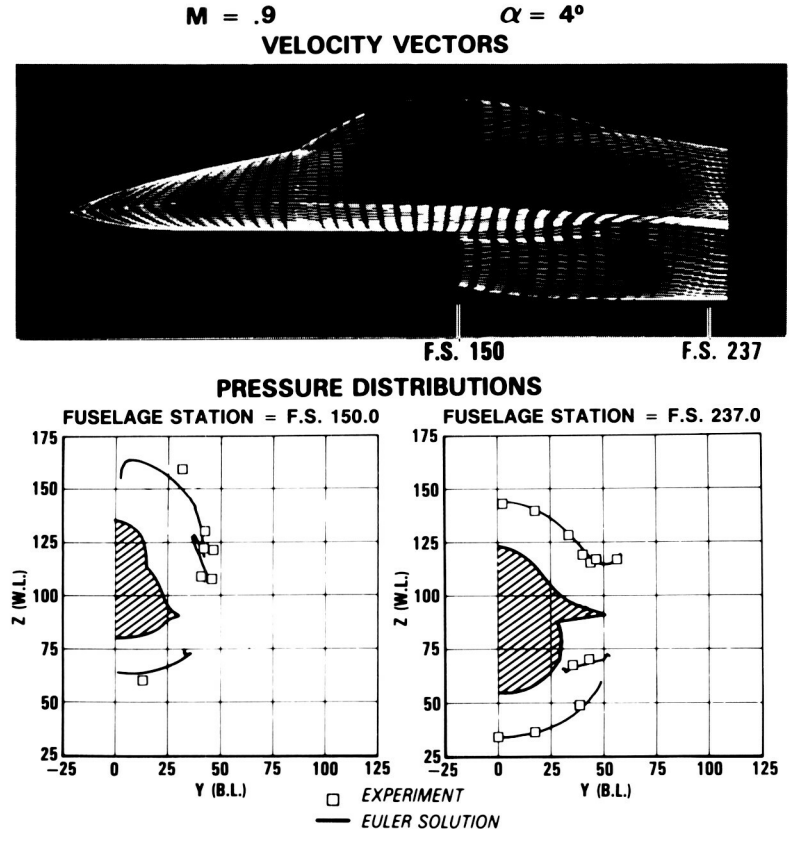

Figure 22. Euler Solution of F-16 Fuselage Flowfield